Top Catal (2009) 52:1566–1574
DOI 10.1007/s11244-009-9289-y

ORIGINAL PAPER

Nitrogen-Containing Carbon Nanostructures as Oxygen-Reduction Catalysts

Elizabeth J. Biddinger · Dieter von Deak · Umit S. Ozkan

Published online: 28 April 2009

Abstract Nitrogen-containing carbon nanostructure (CN_x) catalysts developed by acetonitrile pyrolysis have been studied to better understand their role in the oxygen reduction reaction (ORR) in PEM and direct methanol fuel cell environments. Additional functionalization of the CN_x catalysts with nitric acid has the ability to improve both the activity and selectivity towards ORR.

Keywords CN_x · Nitrogen containing carbon · Oxygen reduction reaction (ORR) · PEM fuel cell cathode · Carbon functionalization

1 Introduction

The incorporation of nitrogen into a carbon matrix has become a widely used method to tailor the structural, chemical and electrical properties of the resulting carbon. Nitrogen behaves as a desirable heteroatom in graphitic carbons because they both can be sp^2 hybridized. The incorporation of nitrogen can increase the electron donation properties of graphite due to nitrogen's higher electronegativity and lone-pair electrons. Even a small amount of nitrogen incorporation (<0.5%) can greatly change electronic transport within a carbon nanotube [1].

Our previous work has included incorporation of nitrogen into carbon nanostructures by pyrolysis of acetonitrile at high temperatures [2–6]. The resulting materials were nitrogen-containing carbon nanostructures (CN_x) and they were used as catalysts for the oxygen reduction reaction (ORR) in PEM and direct methanol fuel cell (DMFC) cathodes [2–8].

The first reports on the use of C–N materials as catalysts for ORR were by Jansinski during the 1960s. These were inspired by the low-temperature oxygen adsorption in hemoglobin, where oxygen is adsorbed on an iron center stabilized by the graphitic nitrogen groups of a macrocycle [9, 10]. These studies focused on the ORR activity of N_4-chelates with cobalt and iron ions as the active centers. This class of catalysts was found to be active for only a limited duration in an acidic fuel cell environment due to catalyst decomposition via hydrolysis in the electrolyte or material degradation caused by peroxide intermediates [3, 4].

In order to stabilize the active macrocycle catalyst Jahnke et al. [11] heat treated macrocycle catalysts in an inert environment. Pyrolysis not only improved the stability of the catalyst, but also enhanced the catalytic activity [4–12]. To create a highly active catalyst, it was found that both nitrogen-containing macrocycles and an electrically conductive support must be present during pyrolysis [13–15]. The increase in activity after pyrolysis was attributed to the formation of more electrically connected active sites through the bonding of macrocycles to the conductive carbon support [12]. Interestingly, the metal component did not necessarily have to be stabilized within the macrocycle precursor. The metal only had to be present among the pyrolysis reactants to create a highly active catalyst [13]. Contrary to the notion that the macrocycle catalyst site remains unaffected, many researchers believe that the active macrocycle center is completely destroyed during pyrolysis and have used electrochemical cyclic voltammetry [14], Mössbauer spectroscopy [15], and X-ray absorption spectroscopy (XAS) [16] to confirm a change in the oxidation state and coordination of the metal species

E. J. Biddinger · D. von Deak · U. S. Ozkan (✉)
Department of Chemical and Biomolecular Engineering, The Ohio State University, Columbus, OH 43210, USA
e-mail: ozkan.1@osu.edu

after pyrolysis. To depart further from macrocycle precursors, a variety of precursors without nitrogen-metal bonds but with simple elemental metal, carbon, and nitrogen containing reactant materials have been pyrolyzed to create active ORR catalysts [19–27].

Although high-temperature treatment of various carbon, nitrogen and metal precursors has been used to create ORR active carbon-nitrogen catalysts and this has shown that it was not necessary to start with macrocycles, the high-temperature treatment overcomes even the highest activation energies making the formation of most carbon-nitride products possible. Since the CN_x ORR catalyst can have nearly any conformation of elemental reactants, the heat treatment confounds the cause of catalytic ORR activity. While it is well established that the nitrogen in carbonaceous materials enhances the catalytic activity for ORR [17], there is still no consensus as to what role it plays. There are two main arguments for how nitrogen enhances ORR in C–N materials; the first is that graphitic nitrogens support the metal in the same manner as metalloporphyrins and the second is the CN_x material has intrinsic catalytic activity of its own accord.

Our work continues to focus on C–N materials, in the form of CN_x catalysts, in an effort to understand the nature of the active sites for ORR. A brief summary of our previous work on CN_x catalysts along with some recent results from our on-going work to further understand and improve the ORR activity of these materials are presented in this paper.

2 Experimental Methods

2.1 Preparation of Catalyst Materials

CN_x catalysts were prepared by acetonitrile pyrolysis over supports of Vulcan Carbon XC-72 (VC), Al_2O_3, SiO_2 and MgO. These supports were used as-received or as-prepared, or were impregnated with Fe, Co or Ni. The preparation methods have been described elsewhere [2–6]. In brief, preparation involved loading the support material into a calcination furnace tube which was heated to 900 °C under nitrogen atmosphere. Acetonitrile-saturated nitrogen gas was introduced at 900 °C for 2 h, then cooled under N_2. The material produced was then washed by either an acid (HF, HCl) or a base (KOH) followed by acid (HCl) to remove the oxide support and any exposed metal particles. After washing, the catalyst was rinsed with 1 L of demineralized, distilled water to remove the wash solution with its dissolved support and metals. The catalyst was then placed in an atmospheric drying oven at 110 °C to drive off the water from washing. The resulting material is considered nitrogen containing carbon nanostructures (CN_x).

To further the study of CN_x catalysts, nitric acid treatments were performed on CN_x materials grown over 2 wt% Fe/MgO. These CN_x catalysts were post treated with agitated concentrated nitric acid (FisherChemical) at 60 °C for 3 h to study any changes in the surface functional groups and the stability of these catalysts in highly acidic media. After concluding the acid treatment, the catalyst was washed with ~1 L total volume of demineralized, distilled water to remove the excess acid solution. The catalyst was then oven dried at 110 °C overnight in air.

2.2 X-ray Photoelectron Spectroscopy (XPS)

The surface species of the catalysts were studied using XPS. A Kratos Ultra Axis Spectrometer was used with a monochromated aluminum anode source for CN_x catalysts supported on SiO_2 and MgO samples, and a Mg anode for CN_x catalysts supported by VC and Al_2O_3. Sensitivity factors reported by the manufacturer based upon the anode type and anode position were used in the calculation of the elemental content in the catalysts.

2.3 Transmission Electron Microscopy (TEM)

The carbon nanostructures were studied using TEM in imaging mode. Catalysts were prepared for imaging by suspending them in ethanol and then depositing the catalyst suspension on lacey-formvar carbon supported on 200 mesh copper TEM grids. An FEI Tecnai F20 XT TEM was used in the analysis.

2.4 Electrochemical Activity and Selectivity Testing

The catalysts developed were tested using the Rotating Ring Disk Electrode (RRDE) half cell technique to determine their activity and selectivity. RRDE inks were prepared fresh for each test. They had a composition of 1:10:160 (by mass) catalyst: 5% Nafion solution (Electrochem): ethanol (Decon). The inks were sonicated for 30 min before being applied to the glassy carbon disk. A catalyst loading of 426 $\mu g/cm^2$ was used with complete dispersion of CN_x in suspension assumed. Testing was performed in 0.5 M H_2SO_4 using an Ag/AgCl(sat KCl) reference electrode and a Pt wire counter electrode. All results in this paper are referenced against the normal hydrogen electrode (NHE). A Princeton Applied Research Bistat connected to a model 636 RRDE set up was used. All cyclic voltammogram (CV) sweeps were performed from 1.2 V to 0.0 V and then to 1.2 V versus NHE. RRDE tests began by saturating the electrolyte with oxygen then running a CV at 10 mV/s on the catalyst coated glassy carbon disk to fully saturate the catalyst pores with electrolyte. The solution was then purged with

argon. Once the system was saturated with Ar, CVs at 50 mV/s were run on the disk paired with Pt ring chronoamperometry set at a constant 1.2 V versus NHE until reproducible current curves were obtained for both the disk and ring to eliminate charging effects. A coulombic charge background scan was then performed under argon saturated electrolyte with the system rotating at 100 rpm while holding the Pt ring at 1.2 V versus NHE and running CV on the disk at 10 mV/s, concurrently. Once the background was collected, the electrolyte solution was then saturated with oxygen again. Catalyst disk CVs at 50 mV/s paired with Pt ring chronoamperometry at 1.2 V versus NHE were performed until steady state currents were reached. The disk (at 10 mV/s) and ring (held at 1.2 V versus NHE) were simultaneously scanned while the electrodes rotated at 100 rpm. At the catalyst disk two main reactions are possible: the desired 4-electron transfer to water

$$O_2 + 4H^+ + 4e^- \rightarrow 2H_2O \qquad 1.23 \text{ V versus NHE [18].}$$

And the undesired 2-electron transfer to hydrogen peroxide

$$O_2 + 2H^+ + 2e^- \rightarrow H_2O_2 \qquad 0.70 \text{ V versus NHE [18].}$$

Additional 10 mV/s CVs in oxygen on the CN_x coated disk were obtained at 0 and 1,000 rpm.

ORR activity was identified as the onset of cathodic current on the catalyst coated glassy carbon electrode during 10 mV/s CVs obtained under oxygen-saturated electrolyte compared to the background current collected under argon-saturated electrolyte.

Selectivity, n, was defined as the average number of electrons transferred for one oxygen molecule, at the catalyst-coated disk for a range of disk potentials. This was determined from the simultaneous measurements taken at the disk and Pt ring at 100 rpm in Ar saturated electrolyte as a background and then compared to the O_2 saturated electrolyte measurements at 100 rpm. H_2O_2 produced on the catalyst coated glassy carbon disk was reduced over the Pt ring according to the following reaction, allowing the calculation of selectivity.

$$H_2O_2 + 2H^+ + 2e^- \rightarrow 2H_2O \qquad 1.76 \text{ V versus NHE [17].}$$

A selectivity of four would represent the complete reduction of oxygen to H_2O whereas, a selectivity of two would indicate partial reduction of oxygen to H_2O_2.

Other techniques including X-ray diffraction (XRD), thermogravimetric analysis (TGA), temperature programmed oxidation experiments (TPO), ^{57}Fe Mössbauer and methanol tolerance testing have been used to characterize the CN_x catalysts and are reported elsewhere [2–8].

3 Results & Discussion

As briefly mentioned in the introduction, a whole body of work involving C–N type catalysts for ORR in acidic media has been reported in the literature over the last half century. While much work has been done, the nature of the activity of these C–N catalysts has yet to be resolved. Some researchers believe that macrocycle center-like sites, where the metal is bound to 2- or 4-N's, is the source of activity [19–22]. Others argue that nitrogen incorporated into the graphitic structure is the source of activity without the presence of a transition metal [23–29] and the role of the metal is limited to catalyzing the growth of the carbon nanostructures with different geometries. Evidence has been reported that support each argument, further increasing the uncertainty in the nature of activity of these C–N ORR catalyst materials. An in-depth review on the literature reports involving the active site debate for C–N ORR catalysts has been published elsewhere [30]. With a better understanding of the nature of the activity of these catalysts, preparation methods could be tailored to increase active sites, thereby increasing the activity of the catalysts and making them more viable for use in commercial fuel cells.

In our prior work, we used classical catalyst characterization techniques along with the electrochemistry required to study such electrocatalysts, in an effort to understand the nature of the active sites in C–N ORR catalysts. More complete details of our previous results can be found in the published literature [2–8].

3.1 CN_x Grown over Vulcan Carbon Supports

Our initial studies involved C–N catalysts prepared by acetonitrile pyrolysis over Vulcan Carbon (VC) supports [6]. The resulting materials developed in the laboratory have been labeled nitrogen containing carbon nanostructures, or CN_x, catalysts for the physical and chemical properties produced through the method. The VC supports were left as received or were impregnated with iron or nickel salts before acetonitrile pyrolysis. Through an optimization study, it was found that metal loadings of 2 wt% on the VC and pyrolysis conditions of 900 °C and for 2 h were ideal for the production of high growth, high surface area catalysts with desirable ORR activity [6].

TEM analysis of the catalysts developed found that CN_x grown over Fe/VC produced many nanofibers with the herringbone-type nanostructure as shown in Fig. 1 [6]. These nanofibers had a high degree of edge plane exposure with the graphitic planes oriented at an angle to the longitudinal axis of the nanofiber. An example of the herringbone nanostructure and other commonly found graphitic carbon nanostructures are illustrated in Fig. 2.

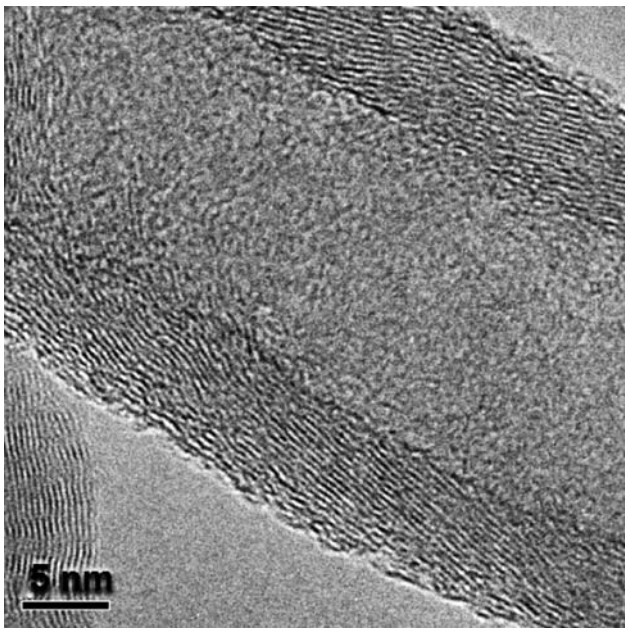

Fig. 1 TEM image of herringbone nanofiber grown over Fe/VC through acetonitrile pyrolysis

The main differences in these nanostructures are the degree of edge-plane exposure and orientation of the graphitic planes in comparison to the longitudinal axis. With CN_x grown over Ni/VC and CN_x over as-received VC, substantial formation of nanostructures with high edge plane exposure was not observed [6].

Temperature-programmed oxidation of these materials showed the formation of NO_x species eluting from the catalysts, indicating that there is significant levels of N present. XPS analysis showed surface nitrogen content as high as 8.6%. The N 1s region of the spectrum could be deconvoluted into three peaks. Figure 3 illustrates the deconvolution of the N 1s region of XPS for both CN_x on Fe/VC and CN_x on Ni/VC [6]. The assignments of the pyridinic-N located on the edge plane of the graphite structure at 398.8 eV and the quarternary-N incorporated deeper in the graphite structure at 401.2 eV are well established in the literature [31, 32]. The assignments of the high binding energy shoulder at 402 eV and above have more possibilities in the literature. One common assignment is the oxygenation of pyridinic-N [31, 32]. Another possible cause of the shoulder is the high-binding energy peak broadening due to the shortening of the bonds with the incorporation of N in the quarternary form in the graphite structure [33]. The locations of the N species described above are illustrated in Fig. 4. The samples grown over iron-containing support had higher pyridinic-N contents, which related well to the greater amount of high-edge-plane exposure of the herringbone nanofibers [6].

Activity testing using half cell methods showed that CN_x grown over Fe/VC had the highest ORR activity [6]. The ORR activity of CN_x on Fe/VC was 315 mV higher than CN_x on VC, 380 mV higher than CN_x on Ni/VC and 525 mV higher than untreated VC [6]. The observation of substantial activity for CN_x grown over as-received VC compared to CN_x on Ni/VC and untreated VC raised further questions about the role of the metal and the role of the pyrolysis step. If iron is a part of the active site, the active site density would have to be very low on these CN_x on VC catalysts, as VC is known to have about 70 ppm iron contamination from the VC manufacturing process. While it has been suggested that this activity is due to the iron contamination [34], the possibility of a metal-free active site seemed plausible with the early results obtained with CN_x grown over as-received VC.

3.2 CN_x Grown over Alumina Supports

The activity results obtained for CN_x grown on as-received VC warranted further investigation into the nature of activity for CN_x catalysts. To probe the ORR activity further, supports without iron contamination were made. A sol–gel alumina with less than 1 ppm transition metal contamination was prepared in the laboratory as a replacement to the VC support [2, 3].

CN_x grown over the as-prepared transition metal free sol–gel alumina were also found to be active for ORR

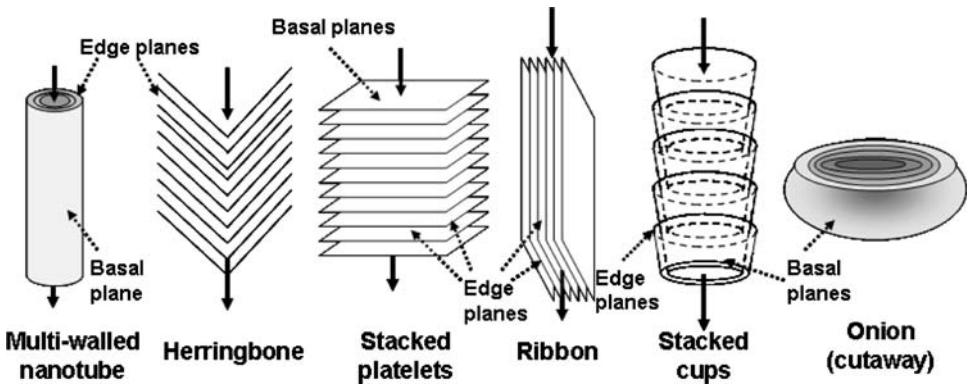

Fig. 2 Types of possible carbon nanostructures with the graphitic basal and edge planes labeled. Sheets illustrated indicate graphitic planes

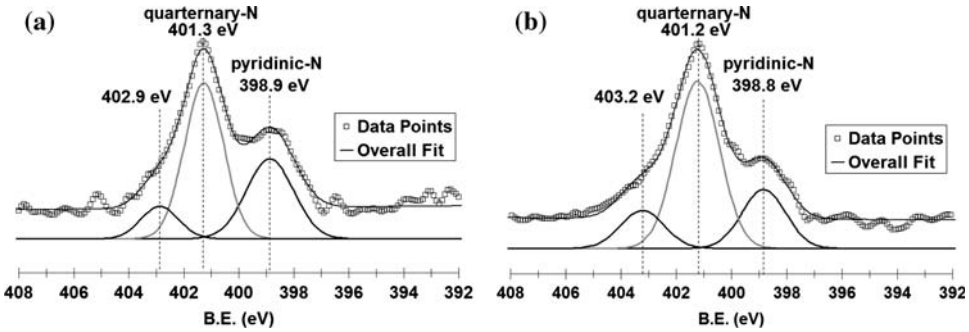

Fig. 3 XPS N 1s region deconvoluted for **a** CN_x grown on Fe/VC, **b** CN_x grown on Ni/VC (Reprinted from [6] with permission from Elsevier)

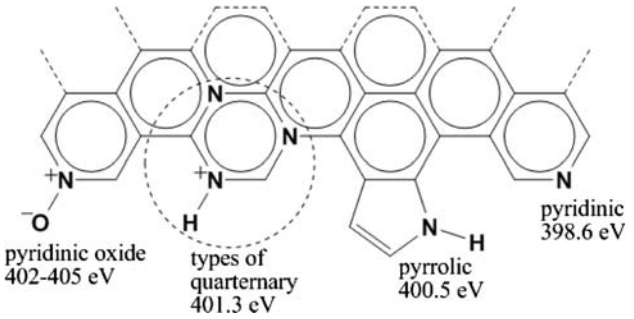

Fig. 4 Types of nitrogen species that can be incorporated into graphitic carbon and the XPS binding energies for each type

when compared to untreated VC and CN_x grown over Ni/VC [2, 3, 6]. This observation supported the hypothesis that the ORR activity for C–N catalysts could be due to an active site, which did not contain a metal. For further comparison, CN_x was grown over supports containing Fe and Ni on Al_2O_3. Once again, it was found that the transition-metal-free CN_x–Al_2O_3 (ORR onset of activity of 675 mV versus NHE) was more active than CN_x on Ni/Al_2O_3 (ORR onset of activity of 570 mV versus NHE) and less active than CN_x on Fe/Al_2O_3 (ORR onset of activity of 740 mV versus NHE) [2, 3].

The use of an oxide support for the formation of an electrocatalyst was a concern because of their low electrical conductivity. For that reason, the alumina was removed from the CN_x catalysts after preparation with a concentrated hydrofluoric acid wash. This also removed any exposed transition metals (if they were included in preparation) from the catalyst. This was verified by XRD [3, 7], TGA-TPO [3] and ^{57}Fe Mössbauer [7]. In addition to removal of the support and exposed metals, the surface area and ORR activity increased after washing [2, 3]. No changes to the carbon nanostructure were observed with washing. For further studies all catalysts made with oxide supports were washed to remove the oxide and exposed metals before characterization or activity testing.

Characterization of the washed CN_x catalysts grown over alumina-containing supports showed that the amount of pyridinic-N in the catalyst increased as the ORR activity increased through analysis with XPS [2, 3]. It was found through TEM imaging of the catalysts that the nanostructures produced were mostly stacked cups with high edge-plane exposure on the most active catalysts (CN_x on Fe/Al_2O_3) further supporting the XPS assignment [2, 3]. CN_x grown over as-prepared alumina was a mixture of nano-onions and stacked cups and CN_x grown over Ni/Al_2O_3 was primarily MWNTs with very little edge plane exposure [2, 3].

Studies with ^{57}Fe Mössbauer over sol–gel alumina doped with Fe were also very informative about the role of Fe in the nano-structure growth mechanism and the nature of Fe at different stages during preparation [7]. Analyses performed over CN_x materials prepared following differing pyrolysis times as well as before or after acid washing provided additional insight. The increase of cementite phase with time of acetonitrile pyrolysis suggested a growth mechanism through a carbide intermediate. The low-temperature (77 K) analysis verified the nature of the metallic iron left behind after washing to be a paramagnetic phase (γ-Fe) which would be stable only if the Fe was encased in graphite. Also, Mössbauer analysis showed no evidence of a N-stabilized Fe center or any correlation of activity with a Fe phase.

After studying the characteristics and activity of the CN_x catalysts grown over alumina supports, several activity hypotheses were supported, including (i) iron is not necessary for ORR activity in C–N catalysts; (ii) pyridinic-N is part of the active site or a marker of ORR activity; (iii) there may be more than one active site for C–N ORR catalysts; and (iv) iron may be a catalyst for the formation of the active site.

3.3 CN_x Grown over SiO_2 and MgO Supports

While study of CN_x grown over alumina supports proved to be very informative for investigation of the activity, the use of hydrofluoric acid wash to dissolve alumina for these catalysts was undesirable due to its inherent exposure

hazards. Alternate supports that could be washed away using more benign chemicals, leaving a concentrated CN_x catalyst, were investigated. Both silica and magnesia supports were found to be satisfactory for the continued study of CN_x ORR catalysts [4, 5]. After pyrolysis, CN_x catalysts grown over SiO_2 were washed with aqueous KOH to remove the oxide support and then with aqueous HCl to remove any exposed metals. CN_x catalysts grown over MgO supports were washed with aqueous HCl to remove both the MgO and the exposed metals.

Characterization and activity testing of both the CN_x catalysts grown over SiO_2 and MgO were found to have similar trends compared to CN_x catalysts grown over Al_2O_3. TEM studies revealed the morphology of CN_x grown over Fe/SiO_2 and Co/SiO_2 to have mostly stacked cup nanostructures [4, 5]. Conversely, CN_x grown over as-received SiO_2 and Ni/SiO_2 lacked significant graphitic nanostructure [4, 5]. For CN_x grown over MgO supports, TEM analysis revealed mostly stacked cup nanofibers for Fe- and Co-impregnated supports. Ni containing supports mostly produced MWNTs. Interestingly, over the as-received MgO only nanocubes were formed. Some nanocubes were also observed over metal-doped MgO support [4, 5].

XPS trends reported for Al_2O_3 supported CN_x were reinforced in MgO and SiO_2 supported CN_x. The amount of pyridinic-N coincided with the amount of stacked cup nanostructure [4, 5]. It was found that for CN_x catalysts grown over both SiO_2 and MgO containing supports the ORR activity was proportional to pyridinic-N content and the amount of stacked cup nanostructure found.

With the results of the work summarized above, CN_x grown over Fe/MgO were used as the base catalyst for future studies that did not specifically investigate transition metal effects. This decision was made based upon the high ORR activity for CN_x grown on Fe/MgO and the ease of removal of the MgO support.

3.4 CN_x Post Treated with HNO_3

Several important questions remain about the CN_x nanostructures and their performance as ORR catalysts. While our previous studies showed a correlation between the pyridinic-N content and ORR activity, it may still be possible to functionalize the graphite surface further through different treatments. There is a large volume of literature on surface functionalization of carbon [34–48] and it may be possible to tailor the surface composition of CN_x materials through such techniques. It is also important to examine the stability of these materials through various treatments in different media. One of the preliminary treatments being investigated in these series of studies involves the concentrated nitric acid post treatment.

Carbons are oxidized to change their hydrophilic properties [35], increase their reactivity [38] and to create anchoring sites for other functional groups or metals [36, 42, 44, 47, 48]. A wide variety of oxygen functional groups can be found on the surface of carbons, depending upon the type of carbon and oxidation treatments. Nitric acid treatments have been used to oxidize carbon [35–38, 40–46]. While nitric acid treatments on carbon have shown an increase in oxygen functional groups, they also led to the addition of more surface nitrogen [43]. Researchers investigating ORR activity for PEM and DMFC ORR catalysts also found that oxidizing carbon containing catalysts aided in the improvement of activity [34, 36–39]. Some of these researchers state that the addition of the oxygen groups to the surface aided in cobalt or iron dispersion for the metal-N–C catalysts being studied [36, 39]. ORR activity was found to be proportional to the oxygen content when nitrogen was not present in the carbon catalyst [34]. When nitrogen and oxygen groups were present on the catalyst surface, they found that nitrogen controlled the ORR activity [34]. It has also been shown that nitrogen incorporation through ammonia treatment on carbon black is much more effective when the carbon has been oxidized with nitric acid first [37]. While some researchers believe that oxygen groups contribute to higher ORR activity through better incorporation of nitrogen and metal particles, some have attributed the ORR activity to quinone/hydroquinone oxygen groups in catalysts which are oxidized carbons containing copper [38]. In these catalysts it is believed that the copper acts as an adsorption site for the oxygen during ORR, but the quinone/hydroquinone site is the actual active site [38].

With the above findings in mind, nitric acid treatments were studied using CN_x grown over Fe/MgO that had been washed with HCl to remove the magnesia and exposed iron. These nitric acid treated catalysts are labeled CN_x–HNO_3 in this study. After 3 h of treatment in concentrated nitric acid, the suspension containing the CN_x and nitric acid was amber in color, suggesting partial removal of carbon tars and amorphous carbons from CN_x. While some carbon was removed, it was not a significant portion. Greater than 90% of the CN_x catalyst mass was collected through the vacuum filtration process.

Significant change to the CN_x nanostructures was not observed when the pre- and post-treated catalysts were studied with TEM. At low magnifications (as shown in Fig. 5a and c), the nanostructure appeared to be consistently stacked cup nanofibers and nanocubes for both the CN_x and CN_x–HNO_3 samples, as expected with CN_x catalysts grown over Fe/MgO. The graphitic planes did not appear to be affected either, as shown in the high-resolution images of Fig. 5b and d.

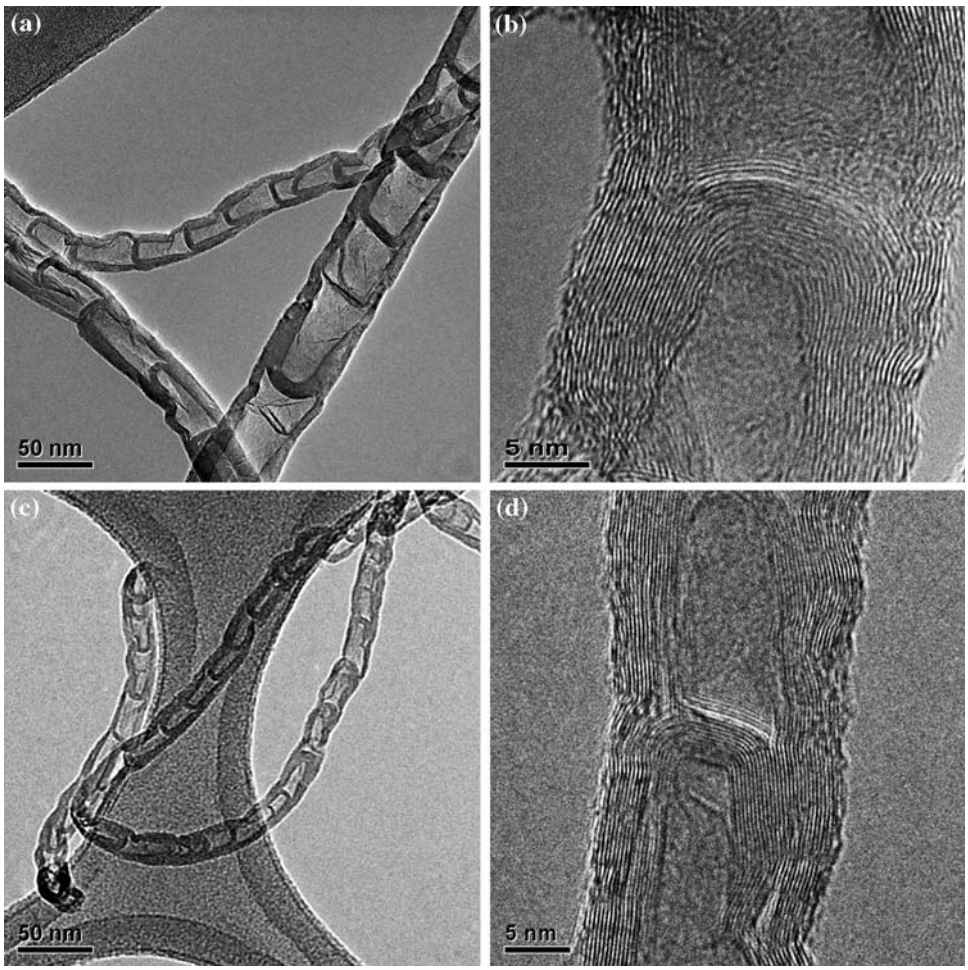

Fig. 5 TEM images of **a** and **b** CN_x grown on Fe/MgO, and **c** and **d** CN_x–HNO_3

While the nanostructure of the CN_x remained intact, the surface species were altered with the nitric acid treatment. Table 1 lists the surface composition of both catalysts as analyzed with XPS. A four-fold increase was observed in oxygen content on the surface of the CN_x–HNO_3 catalyst. This is consistent with other studies involving surface oxidation with nitric acid. The O 1s region spectra did not change appreciably with the nitric acid treatment, suggesting that CN_x catalysts already contain a similar distribution of oxygen species compared to CN_x treated with HNO_3. The nitric acid treatment only appeared to increase the quantity of oxygen on the surface. While the table indicates that the portion of the surface attributed to nitrogen decreases slightly with nitric acid treatment, the ratio of N to C remains constant. The pyridinic-N component of the N 1s region increased from 24.1% to 28.8% with nitric acid treatment.

Table 1 Surface species (atomic %) on CN_x and CN_x–HNO_3 from XPS analysis

	CN_x	CN_x–HNO_3
O 1s	1.5	6.5
N 1s (total)	7.7	7.2
Pyridinic (portion of N)	24.1	28.8
C 1s	90.8	86.3

The combined retention of nanostructure, increase in oxygen surface content, and increase in pyridinic-N, appeared to result in an overall increase in the catalytic performance of the CN_x–HNO_3 catalyst. As shown in Fig. 6, the ORR activity for CN_x–HNO_3 increased both in onset of activity and current density. In addition, the selectivity, as illustrated in the inset to Fig. 6, significantly improved as well. Further treatments and characterization of the CN_x–HNO_3 catalyst are required to better determine the impact of each effect on the improved activity and selectivity as well as any synergetic effects.

4 Conclusions

Nitrogen containing carbon nanostructured (CN_x) catalysts have been investigated in a series of studies to better

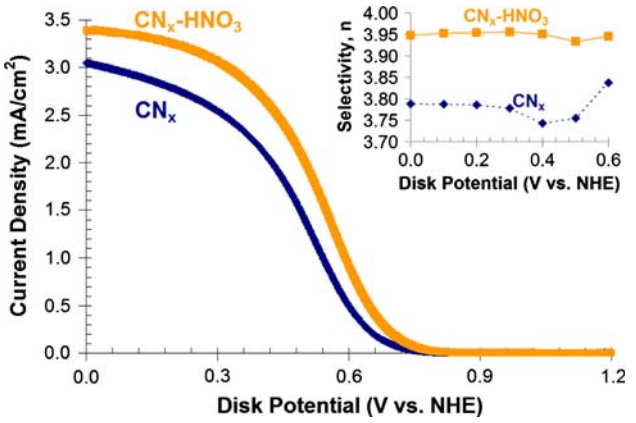

Fig. 6 Comparison of ORR activity for CN_x and CN_x–HNO_3 measured using RRDE at 1,000 rpm. Inset: Selectivity of CN_x and CN_x–HNO_3

understand the nature of the activity for ORR in the fuel cell environment. Results from these studies suggest that iron does not have to be the center or even a component of the ORR active site, but possibly plays a role in the formation of the active site through the carbon nanostructure growth mechanism. Pyridinic-N and the degree of graphitic edge plane exposure of the catalyst appear to play a role in the activity of the ORR catalysts.

Post-treating CN_x catalysts has the potential to further improve the ORR activity and selectivity while enhancing the understanding of what properties make a good non-noble metal ORR catalyst. It has been shown that post treating CN_x with concentrated nitric acid improves ORR activity and selectivity. Further characterization and additional surface functionalization treatments on the CN_x–HNO_3 catalysts are ongoing. Additional treatments to both CN_x and non-nitrogen containing carbon nanostructures have the potential to aid in the understanding of the role that surface functional groups and heteroatoms play in CN_x ORR catalysts.

Acknowledgments Financial support provided for this work by the Department of Energy-Basic Energy Sciences (DE-FG02-07ER15896) and the National Science Foundation (CTS-0437451) is gratefully acknowledged. Authors also acknowledge the support provided by the Ohio Department of Development through the Wright Center of Innovation for Fuel Cells.

References

1. Latil S, Roche S, Mayou D, Charlier J-C (2004) Phys Rev Lett 92:256805
2. Matter PH, Ozkan US (2006) Catal Lett 109:115
3. Matter PH, Wang E, Arias M, Biddinger EJ, Ozkan US (2006) J Phys Chem B 110:18374
4. Matter PH, Wang E, Arias M, Biddinger EJ, Ozkan US (2007) J Mol Catal 264:73
5. Matter PH, Wang E, Ozkan US (2006) J Catal 243:395
6. Matter PH, Zhang L, Ozkan US (2006) J Catal 239:83
7. Matter PH, Wang E, Millet J-MM, Ozkan US (2007) J Phys Chem C 111:1444
8. Biddinger EJ, Ozkan US (2007) Top Catal 46:339
9. Jansinski R (1964) Nature 201:1212
10. Jansinski R (1965) J Electrochem Soc 112:526
11. Jahnke H, Schonborn M, Zimmerman G (1976) Fortschr Chem Forsch 61:133
12. van Veen JAR, van Baar JF, Kroese KJ (1981) Chem Soc Faraday Trans I 77:2827
13. Kaisheva A, Gamburtsev S, Iliev I (1982) Sov J Electrochem 18:127
14. Gojkovic SL, Gupta S, Savinell RF (1998) J Electrochem Soc 145:3493
15. Scherson DA, Gupta SL, Fierro C, Yeager EB, Kordesch ME, Eldridge J, Hoffman RW, Blue J (1983) Electrochim Acta 28:1205
16. Martins Alves MC, Dodelet JP, Guay D, Ladouceur M, Tourillon G (1992) J Phys Chem 96:10898
17. Shao Y, Sui J, Yin G, Gao Y (2008) Appl Catal B 79:89
18. Bard AJ, Faulkner LR (2001) Electrochemical methods: fundamentals and applications. Wiley, New York
19. Yeager E (1986) J Mol Catal 38:5
20. Lefevre M, Dodelet JP, Bertrand P (2002) J Phys Chem B 106:8705
21. Jaouen F, Lefevre M, Dodelet J-P, Cai M (2006) J Phys Chem B 110:5553
22. Bouwkamp-Wijnoltz AL, Visscher W, van Veen JAR, Boellaard E, van der Kraan AM, Tang SC (2002) J Phys Chem B 106:12993
23. Wiesener K (1986) Electrochim Acta 31:1073
24. Gojkovic S, Gupta S, Savinell R (1999) J Electroanal Chem 462:63
25. Gouerec P, Biloul A, Contamin O, Scarbeck G, Savy M, Riga J, Weng LT, Bertrand P (1997) J Electroanal Chem 422:61
26. Maldonado S, Stevenson KJ (2004) J Phys Chem B 108:11375
27. Maldonado S, Stevenson KJ (2005) J Phys Chem B 109:4707
28. Nallathambi V, Lee J-W, Kumaraguru SP, Wu G, Popov BN (2008) J Power Sources 183:34
29. Wang P, Ma Z, Zhao Z, Jia L (2007) J Electroanal Chem 611:87
30. Matter PH, Biddinger EJ, Ozkan US (2007) In: Spivey JJ (ed) Catalysis, vol 20. The Royal Society of Chemistry, Cambridge, UK, p 338
31. Pels JR, Kapteijn F, Moulijn JA, Zhu Q, Thomas KM (1995) Carbon 33:1641
32. van Dommele S, Romero-Izquirdo A, Brydson R, de Jong KP, Bitter JH (2008) Carbon 46:138
33. Casanovas J, Ricart JM, Rubio J, Illas F, Jimenez-Mateos JM (1996) J Am Chem Soc 118:8071
34. Jaouen F, Marcotte S, Dodelet J-P, Lindbergh G (2003) J Phys Chem B 107:1376
35. Ros TG, van Dillen AJ, Geus JW, Koningsberger DC (2002) Chemistry 8:1151
36. Subramanian NP, Kumaraguru SP, Colon-Mercado H, Kim H, Popov BN, Black T, Chen DA (2006) J Power Sources 157:56
37. Wang H, Cote R, Faubert G, Guay D, Dodelet JP (1999) J Phys Chem B 103:2042
38. Nabae Y, Yamanaka I, Otsuka K (2005) Appl Catal A-Gen 280:149
39. Gouerec P, Savy M, Riga J (1998) Electrochim Acta 43:743
40. Figueiredo JL, Pereira MFR, Freitas MMA, Orfao JJM (1999) Carbon 37:1379
41. Wu Z, Pittman CU Jr, Gardner SD (1995) Carbon 33:597

42. Rasheed A, How JY, Dadmun MD, Britt PF (2007) Carbon 45:1072
43. Xia W, Wang Y, Bergstraber R, Kundu S, Muhler M (2007) Appl Surf Sci 254:247
44. Takoaka M, Yokokawa H, Takeda N (2007) Appl Catal B 74:179
45. Frysz CA, Chung DDL (1997) Carbon 35:1111
46. Krishnankutty N, Vannice MA (1995) Chem Mater 7:754
47. Guha A, Lu W, Zawodzinski TA Jr, Schiraldi DA (2007) Carbon 45:1506
48. Natarajan SK, Cossement D, Hamelin J (2007) J Electrochem Soc 154:B310